

Crystal structures of spin-Jahn-Teller-ordered MgCr_2O_4 and ZnCr_2O_4

Moureen C. Kemei,^{1,*} Phillip T. Barton,¹ Stephanie L. Moffitt,¹ Michael W. Gaultois,¹
Joshua A. Kurzman,¹ Ram Seshadri,¹ Matthew R. Suchomel,² and Young-Il Kim³

¹*Materials Department and Materials Research Laboratory
University of California, Santa Barbara, CA, 93106, USA*

²*X-Ray Science Division and Material Science Division
Argonne National Laboratory, Argonne IL, 60439, USA*

³*Department of Chemistry, Yeungnam University
Gyeongsan, Gyeongbuk 712-749, Korea*

(Dated: March 6, 2013)

Magnetic ordering in the geometrically frustrated magnetic oxide spinels MgCr_2O_4 and ZnCr_2O_4 is accompanied by a structural change that helps relieve the frustration. Analysis of high-resolution synchrotron X-ray scattering reveals that the low-temperature structures are well described by a two-phase model of tetragonal $I4_1/amd$ and orthorhombic $Fddd$ symmetries. The Cr_4 tetrahedra of the pyrochlore lattice are distorted at these low-temperatures, with the $Fddd$ phase displaying larger distortions than the $I4_1/amd$ phase. The spin-Jahn-Teller distortion is approximately one order of magnitude smaller than is observed in first-order Jahn-Teller spinels such as NiCr_2O_4 and CuCr_2O_4 . In analogy with NiCr_2O_4 and CuCr_2O_4 , we further suggest that the precise nature of magnetic ordering can itself provide a second driving force for structural change.

PACS numbers: 61.50.Ks, 75.50.Ee, 75.50.Lx

The ACr_2O_4 spinels possess highly degenerate spin liquid states that can order at low temperature in conjunction with a lattice distortion, in a manner sometimes referred to as spin-Jahn-Teller ordering.[1, 2] Despite extensive studies of the spin-Jahn-Teller phases of ACr_2O_4 spinels, there is little agreement on the full description of the low-temperature structures of MgCr_2O_4 and ZnCr_2O_4 . [3, 4] At room temperature, ACr_2O_4 are cubic spinels in the space group $Fd\bar{3}m$, provided the A ions are non-magnetic. A cations occupy tetrahedral sites while Cr^{3+} with spin $S = 3/2$ populate octahedral sites. These are normal spinels: Cr^{3+} shows a strong preference for the octahedral site.[5] Magnetic frustration in ACr_2O_4 spinels is known to decrease from $A = \text{Zn}$ to Mg to Cd to Hg with the respective spinels showing Weiss intercepts Θ_{CW} of -390 K,[6] -346 K,[6, 7] -71 K,[6] and -32 K[6, 8] and spin-Jahn-Teller ordering temperatures (T_N) of ≈ 12.7 K,[9] ≈ 12.5 K,[1] ≈ 7.8 K,[10–12] and ≈ 5.8 K[8].

Several low-temperature nuclear structures have been proposed for ACr_2O_4 spinels. X-ray diffraction studies reveal $Fddd$ symmetry in the spin-Jahn-Teller phase of HgCr_2O_4 . [8] A tetragonal $I4_1/amd$ structure of MgCr_2O_4 was identified in low-temperature synchrotron X-ray[13] and neutron powder diffraction studies.[9] A tetragonal distortion has also been observed in the antiferromagnetic phase of CdCr_2O_4 , identified by Aguilar *et al.* using infrared spectroscopy,[12] and by Chung and co-workers from elastic and inelastic neutron scattering studies.[11] The low-temperature structure of CdCr_2O_4 was assigned to the $I4_1/amd$ space group as reported by Lee *et al.* from synchrotron X-ray and neutron scattering studies of single crystals.[3] In the same report, single crystals of ZnCr_2O_4 were reported to adopt the tetrag-

onal $I\bar{4}m2$ space group below the Néel temperature.[3] However, X-ray powder diffraction by Kagomiya *et al.* suggested, without describing the complete structure, that at low-temperatures ZnCr_2O_4 is modelled by the orthorhombic space group $Fddd$. [4] Recent electron-spin resonance studies of single crystal ZnCr_2O_4 by Glazkov *et al.* showed that tetragonal and orthorhombic distortions coexist in the Néel phase of ZnCr_2O_4 . [14] In this Letter, we report coexisting tetragonal $I4_1/amd$ and orthorhombic $Fddd$ symmetries in the spin-Jahn-Teller phases of MgCr_2O_4 and ZnCr_2O_4 , observed using high-resolution synchrotron X-ray powder diffraction. Phase coexistence is suggested for the first time in these materials from diffraction studies.

MgCr_2O_4 was prepared by calcination of appropriate solution mixtures of the nitrates $\text{Mg}(\text{NO}_3)_2 \cdot 6\text{H}_2\text{O}$ and $\text{Cr}(\text{NO}_3)_3 \cdot 9\text{H}_2\text{O}$ at 1000°C for 10 hours. ZnCr_2O_4 and CdCr_2O_4 were prepared by solid-state methods from ZnO , CdO , and Cr_2O_3 powders. Samples were annealed in the temperature range 800°C to 1100°C . A separate ZnCr_2O_4 sample was prepared in a Pt crucible by heating ZnO in an excess $\text{K}_2\text{Cr}_2\text{O}_7$ flux at 800°C for 24 hours, followed by cooling at 15°C/hr to room temperature. Samples were structurally characterized by high-resolution ($\Delta Q/Q \leq 2 \times 10^{-4}$) synchrotron X-ray powder diffraction at temperatures between 6 K and 295 K. These measurements were performed at beamline 11-BM of the Advanced Photon Source, Argonne National Laboratory. Structural models were refined against diffraction data using the Rietveld method as implemented in the EXPGUI/GSAS software program.[15, 16] Atom positions for the low-symmetry structures were obtained using the internet-server tool ISODISPLACE.[17] Crystal distortions were analyzed using the program VESTA.[18]

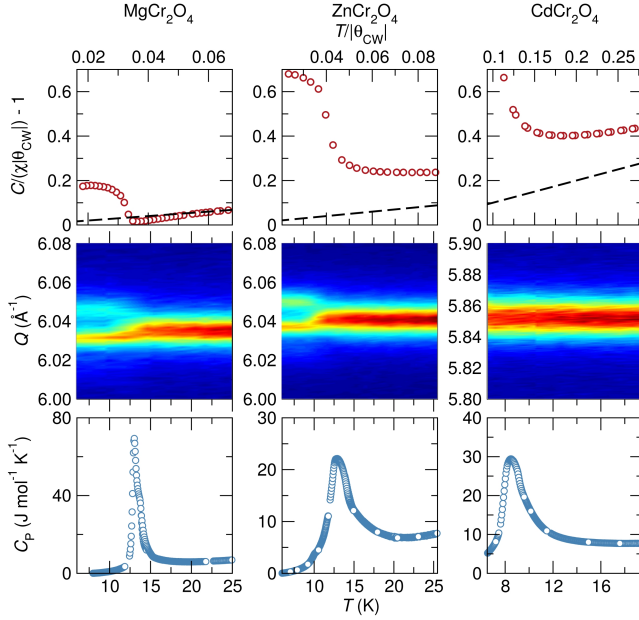


FIG. 1: (Color online) Spin-Jahn-Teller distortions in ACr_2O_4 spinels. The top panel shows the scaled inverse field-cooled susceptibility. The dashed black line models ideal paramagnetism. $MgCr_2O_4$ and $ZnCr_2O_4$ were measured under a 1000 Oe field while $CdCr_2O_4$ was measured in 6000 Oe. Antiferromagnetic order is suppressed to low temperatures in $MgCr_2O_4$ ($T_N = 12.9$ K), $ZnCr_2O_4$ ($T_N = 12.3$ K), and $CdCr_2O_4$ ($T_N = 7.86$ K). The splitting of high-symmetry cubic diffraction peaks into several low-symmetry peaks shows the onset of spin-driven structural distortions (middle panel). $CdCr_2O_4$ shows a subtle structural distortion that is indicated by a slight decrease in intensity and increase in width of the high-symmetry peak. The bottom panel shows the change in entropy at the Néel temperature.

TABLE I: Magnetic parameters of ACr_2O_4 spinels

	T_N (K)	Θ_{CW} (K)	$f = \frac{ \Theta_{CW} }{T_N}$	μ_{exp} (μ_B)	μ_{calc} (μ_B)
$MgCr_2O_4$	12.9	-368	29	5.4	5.47
$ZnCr_2O_4$	12.3	-288	23	5.2	5.47
$CdCr_2O_4$	7.86	-69.7	8.9	5.3	5.47

Magnetic properties were characterized using a Quantum Design MPMS 5XL superconducting quantum interference device (SQUID). Heat capacity measurements were performed using a Quantum Design Physical Properties Measurement System.

At room temperature, the prepared ACr_2O_4 spinels are single phase homogeneous compounds in the space group $Fd\bar{3}m$ with lattice parameters 8.33484(8) Å for $MgCr_2O_4$ and 8.32765(8) Å for $ZnCr_2O_4$; $MgCr_2O_4$ has a Cr_2O_3 impurity of 3.0 wt.%. The $ZnCr_2O_4$ sample prepared from $K_2Cr_2O_7$ flux has the cubic lattice constant 8.3288(2) Å. The cell parameters are in good agreement with previous reports.[9] Scaled inverse field-cooled susceptibilities of ACr_2O_4 as described by the re-

cast Curie-Weiss equation are shown in the top panel of Fig. 1.[19] Antiferromagnetic ordering occurs when $T/\Theta_{CW} \ll 1$, indicating geometrically frustrated spin interactions (top axis scale of Fig. 1). Slight antiferromagnetic spin correlations are observed above T_N in $ZnCr_2O_4$ and $CdCr_2O_4$. We define T_N as the temperature at which $d\chi_{ZFC}/dT$ is maximized. Magnetic properties of $MgCr_2O_4$ and $ZnCr_2O_4$ are extremely sensitive to non-stoichiometry.[20] The magnetic properties of the samples presented here are tabulated in Table I and are in good agreement with earlier reports of highly stoichiometric compounds.[19, 20] Experimental magnetic moments of these compounds are within error of the calculated effective moment of $5.47\mu_B$ (Table I). There is a ≈ 0.3 K thermal hysteresis between the zero-field-cooled and field-cooled temperature dependent susceptibilities of the ACr_2O_4 spinels. We observe a Θ_{CW} of -288 K for $ZnCr_2O_4$ which is consistent with the earlier work by Melot *et al.*[19] but is lower than other Θ_{CW} values reported in the literature.[7, 9] The magnetic ordering transitions of ACr_2O_4 spinels are associated with changes in entropy (Figure 1) and this agrees well with the earlier work of Klemme *et al.*[21, 22] $ZnCr_2O_4$ and $CdCr_2O_4$ have smooth heat capacity anomalies while $MgCr_2O_4$ has a sharp anomaly with a shoulder feature that could indicate that its structural and magnetic transitions occur at slightly different temperatures.

The cubic $Fd\bar{3}m$ (800) diffraction peak of $MgCr_2O_4$ and $ZnCr_2O_4$ splits into several low-symmetry peaks (Figure 1). $CdCr_2O_4$ on the other hand, while displaying some peak broadening, remains well modelled by the high-temperature $Fd\bar{3}m$ space group even at 6.9 K (Figure 1). Rietveld fits to the low-temperature synchrotron X-ray powder diffraction data of $MgCr_2O_4$ and $ZnCr_2O_4$ using structural models reported in the literature[3, 4, 9, 13] resulted in regions of poorly fit intensity. Similarly, the low-symmetry structures $F222$, $C2/c$, and $I2/a$ could not model the data well. Group-subgroup relations of the space group $Fd\bar{3}m$ yield the lower-symmetry groups $I4_1/amd$ and $Fddd$. Individually, neither of these structural models can reproduce the intensities and peak splittings observed in our low-temperature diffraction patterns of $MgCr_2O_4$ and $ZnCr_2O_4$. However, we find that the diffraction data can be well described by a two-phase model combining both tetragonal $I4_1/amd$ and orthorhombic $Fddd$ structures [Fig. 2(a)]. This refinement yields chemically reasonable and stable isotropic thermal displacement parameters for both phases (Table II). In Fig. 2(b), the low-temperature peak splitting of the cubic $Fd\bar{3}m$ (800) reflection is deconvoluted into contributions from the $I4_1/amd$ and $Fddd$ phases.

Nearly equal fractions of the two phases coexist in the low-temperature nuclear structures of $MgCr_2O_4$ and $ZnCr_2O_4$ [Figure 2(c)]. Employing the Thompson-Cox-Hastings pseudo-voigt profile function, we observe a slight increase of the $Fddd$ phase fraction with a de-

TABLE II: The low-temperature structures of MgCr_2O_4 and ZnCr_2O_4 as determined from Rietveld refinement of high-resolution synchrotron X-ray powder diffraction data. All atomic parameters were allowed to vary during the structural refinement except for isotropic thermal parameters that are constrained to be the same for both low-temperature phases.

	MgCr_2O_4	ZnCr_2O_4	$\text{ZnCr}_2\text{O}_4^a$
T (K)	5.7	5.4	6.9
λ (Å)	0.413393	0.413399	0.413331
space group	$I4_1/amd$	$I4_1/amd$	$I4_1/amd$
Z	4	4	4
a (Å)	5.89351(2)	5.88753(1)	5.88919(2)
c (Å)	8.31503(7)	8.30895(4)	8.31703(5)
Vol (Å ³)	288.809(2)	288.013(2)	288.456(2)
Mg/Zn	$(0, \frac{3}{4}, \frac{1}{8})$	$(0, \frac{3}{4}, \frac{1}{8})$	$(0, \frac{3}{4}, \frac{1}{8})$
Cr	$(0, 0, \frac{1}{2})$	$(0, 0, \frac{1}{2})$	$(0, 0, \frac{1}{2})$
O	0	0	0
	0.5240(3)	0.5250(4)	0.5196(5)
	0.7391(2)	0.7379(4)	0.7387(5)
	0.42(0)	0.43(0)	0.39(0)
wt. frac.			
^b coherence length(nm)	69.9	74.5	
space group	$Fddd$	$Fddd$	$Fddd$
Z	8	8	8
a (Å)	8.3041(2)	8.3012(1)	8.3059(9)
b (Å)	8.3228(2)	8.3144(1)	8.3247(8)
c (Å)	8.3526(2)	8.3430(1)	8.3415(0)
Vol (Å ³)	577.279(6)	575.830(5)	576.758(4)
Mg/Zn	$(\frac{1}{8}, \frac{1}{8}, \frac{1}{8})$	$(\frac{1}{8}, \frac{1}{8}, \frac{1}{8})$	$(\frac{1}{8}, \frac{1}{8}, \frac{1}{8})$
Cr	$(\frac{1}{2}, \frac{1}{2}, \frac{1}{2})$	$(\frac{1}{2}, \frac{1}{2}, \frac{1}{2})$	$(\frac{1}{2}, \frac{1}{2}, \frac{1}{2})$
O	0.26130(4)	0.26466(4)	0.26092(3)
	0.26135(4)	0.25722(7)	0.26639(5)
	0.26093(2)	0.26193(5)	0.26015(3)
wt. frac.	0.55(0)	0.57(0)	0.61(0)
^b coherence length(nm)	40.4	35.6	
Mg/Zn U_{iso}	0.00290(1)	0.00254(5)	0.00305(4)
Cr U_{iso}	0.00167(4)	0.00074(5)	0.00164(4)
O U_{iso}	0.00115(1)	0.00458(2)	0.00321(2)
χ^2	2.903	3.673	1.709
R_{wp}	0.0331	0.0582	0.0823

^a ZnCr_2O_4 prepared from a flux of $\text{K}_2\text{Cr}_2\text{O}_7$

^bDetermined from Scherrer analysis of well resolved peaks. This is the lower limit of crystallite size and assumes that all peak broadening is due to crystallite size

crease in temperature below T_N for both MgCr_2O_4 and ZnCr_2O_4 . While the estimated standard deviations suggest rather accurate phase fractions (Table II), separate refinements employing different profile functions show variations of up to 10%. Scherrer analysis of deconvoluted $I4_1/amd$ and $Fddd$ peaks shown in Fig. 2(b) yield larger coherence lengths in the tetragonal phases of MgCr_2O_4 and ZnCr_2O_4 compared with the orthorhombic phases (Table II). Williamson–Hall analysis yields room temperature crystallite sizes of 118 nm in MgCr_2O_4 and 200 nm in ZnCr_2O_4 . The analysis reveals that larger $Fd\bar{3}m$ domains split into smaller domains of coexisting $I4_1/amd$ and $Fddd$ phases (Table II). The two low-temperature phases coexist down to the lowest tempera-

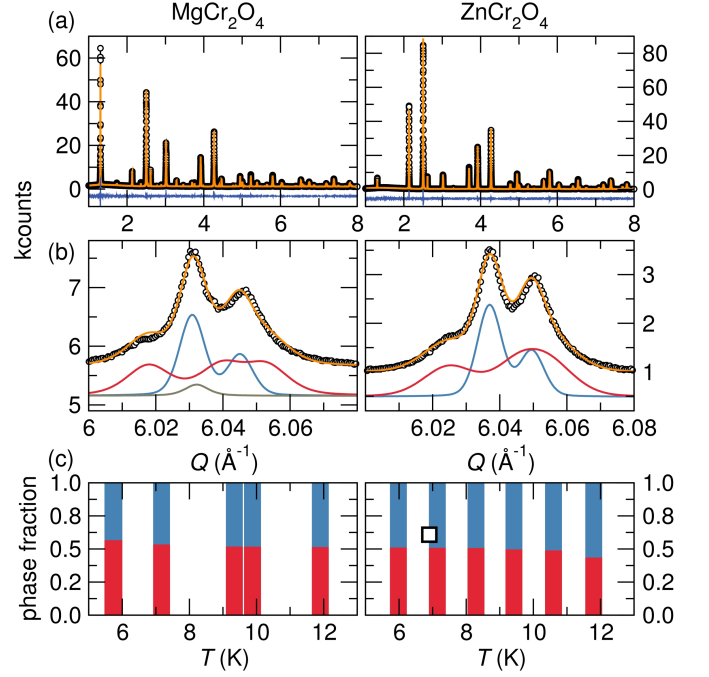


FIG. 2: (Color online) Low-temperature diffraction and Rietveld refinement of MgCr_2O_4 (left panel) and ZnCr_2O_4 (right panel). (a) High-resolution synchrotron X-ray powder patterns collected at ≈ 6 K and indexed to a two-phase model of tetragonal $I4_1/amd$ and orthorhombic $Fddd$ symmetries [Data (black), combined $I4_1/amd$ and $Fddd$ fit (orange), difference (blue)]. (b) The high-symmetry (800) peak splits into several $I4_1/amd$ and $Fddd$ reflections. The $I4_1/amd$ and $Fddd$ fits have been offset from the data for clarity. [$I4_1/amd$ (blue), $Fddd$ (red), and Cr_2O_3 impurity (grey)] (c) Nearly equal amounts of $I4_1/amd$ (blue) and $Fddd$ (red) phases coexist below T_N ; the $Fddd$ phase fraction increases slightly with decreasing T . The sample of ZnCr_2O_4 prepared using $\text{K}_2\text{Cr}_2\text{O}_7$ flux shows a similar low-temperature structure and its phase fractions are indicated by the square.

tures studied.

We have also examined a ZnCr_2O_4 sample prepared in a $\text{K}_2\text{Cr}_2\text{O}_7$ flux to explore the effect of sample preparation conditions. High-resolution synchrotron X-ray diffraction measurements carried out at 7 K reveal that it is also described by a combination of both $I4_1/amd$ and $Fddd$. There are subtle differences in the low-temperature phase composition of the flux-prepared sample. Specifically, a slightly higher $Fddd$ phase fraction is observed compared to the sample prepared by solid state methods [Figure 2(c)].

The $Fd\bar{3}m$ lattice parameter of MgCr_2O_4 and ZnCr_2O_4 splits abruptly into two $I4_1/amd$ and three $Fddd$ lattice constants at T_N , as shown in Fig. 3(a) and (c) respectively. The $Fddd$ a and c parameters of MgCr_2O_4 and ZnCr_2O_4 show the greatest distortion from cubic symmetry. The $Fddd$ phase of each compound has a smaller volume than its $I4_1/amd$ counterpart, suggesting that $Fddd$ is the lower energy structure.

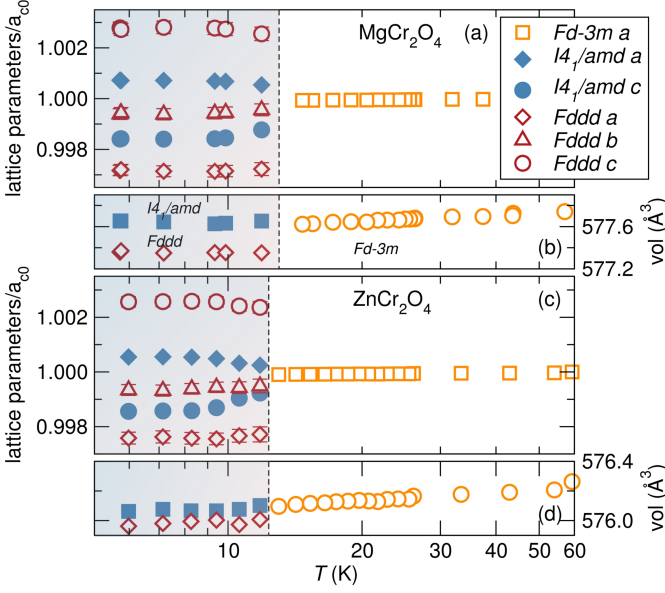


FIG. 3: (Color online) Temperature evolution of lattice parameters in MgCr_2O_4 and ZnCr_2O_4 through their magnetostructural distortions. The cubic lattice constants of MgCr_2O_4 (a) and ZnCr_2O_4 (c) separate into $I4_1/amd$ and $Fddd$ lattice constants at $T_N = 12.9$ K and $T_N = 12.3$ K respectively. The lattice parameters of MgCr_2O_4 are normalized by the lattice constant at 57.1 K ($a_{c0} = 8.32871$ Å) while the lattice constants of ZnCr_2O_4 are normalized by the lattice constant at 59.3 K ($a_{c0} = 8.3216$ Å). The $I4_1/amd$ lattice constants have been multiplied by $\sqrt{2}$. A change in slope of the cell volumes of MgCr_2O_4 (b) and ZnCr_2O_4 (d) occurs at their respective T_N . In some cases, error bars are smaller than the symbols.

MgCr_2O_4 and ZnCr_2O_4 undergo a first-order structural transition at T_N indicated by the change in slope of the cell volume [Figure 3(b) and (d)], the onset of a two-phase regime [Figure 2(b)], and the release of entropy (Figure 1).

The Cr_4 tetrahedra of MgCr_2O_4 and ZnCr_2O_4 are distorted below T_N . We compute a tetrahedral distortion index of Cr_4 tetrahedra, $D = 1/n \sum_{i=1}^n (l_i - \bar{l})/\bar{l}$, where l_i is the i th Cr-Cr bond distance and \bar{l} is the average Cr-Cr bond distance.[23] A larger D is seen for the $Fddd$ phases of MgCr_2O_4 and ZnCr_2O_4 in comparison to the $I4_1/amd$ phases [Figure 4(a)]. Similarly, we compute an angle variance of Cr_4 tetrahedra, $\sigma^2 = 1/(m-1) \sum_{i=1}^m (\phi_i - \phi_0)^2$, where ϕ_0 is the ideal tetrahedron angle of 109.47° , ϕ_i is the measured angle, and m is (the number of faces of a tetrahedron) $\times 3/2$. [18, 24] A greater angle variance occurs in the orthorhombic phases of MgCr_2O_4 and ZnCr_2O_4 rather than in the tetragonal phases. The ZnCr_2O_4 sample prepared from a $\text{K}_2\text{Cr}_2\text{O}_7$ flux has less distortion of its Cr_4 tetrahedra compared with the solid state ZnCr_2O_4 compound. Of the two compounds studied, the Cr_4 tetrahedra are more distorted in MgCr_2O_4 than in ZnCr_2O_4 .

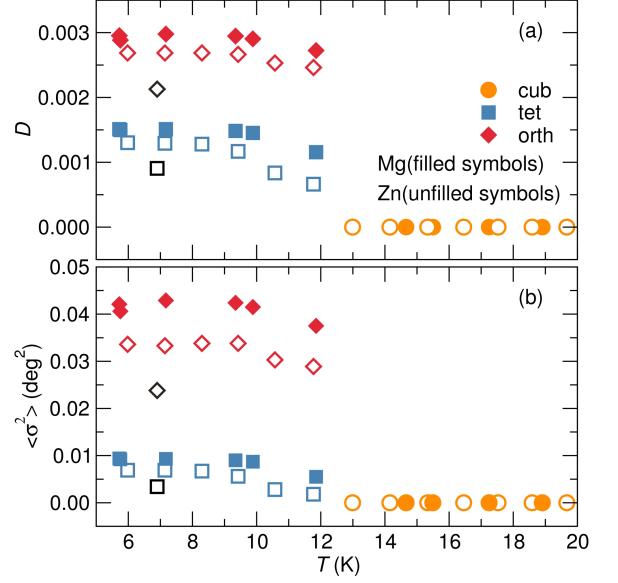


FIG. 4: (Color online) Distortion of Cr_4 tetrahedra in the spin-Jahn-Teller phases of MgCr_2O_4 and ZnCr_2O_4 . (a) At 12.9 K and 12.3 K, Cr-Cr bond distance distortions occur in MgCr_2O_4 and ZnCr_2O_4 respectively. (b) Distortion of Cr_4 angles occur below T_N in MgCr_2O_4 and ZnCr_2O_4 . The black symbols show distortions in the ZnCr_2O_4 sample prepared from a $\text{K}_2\text{Cr}_2\text{O}_7$ flux.

The spin-Jahn-Teller distortion of MgCr_2O_4 and ZnCr_2O_4 resembles martensitic phase transitions, which are displacive solid-solid transitions. These transformations can be induced by varying temperature, involve changes in crystal symmetry without a change in chemical composition, and show hysteresis. Volume changes between the parent and product phases that occur at the spin-Jahn-Teller distortion temperature could induce strains that result in a biphasic product.

It is important to consider whether a single low-symmetry space group could model the data. Our refinements using $F222$, $C2/c$, or $I2/a$ were unable to generate the observed peak separations. Analysis of the Cr_4 tetrahedra distortions shows that the $Fddd$ phase is more distorted than the $I4_1/amd$ phase. Additionally, the $Fddd$ phase fraction increases slightly with a decrease in temperature below T_N . The combination of these two effects would be challenging to describe using a single low-symmetry structural model. Further, the two-phase $I4_1/amd$ and $Fddd$ model is robust against changes in sample preparation conditions.

Phase coexistence following a phase transition is not unusual. Compositional inhomogeneity contributes to multiple low-temperature phases in $\text{Nd}_{0.5}\text{Sr}_{0.5}\text{MnO}_3$. [25] Similarly, complex phase behavior featuring three coexisting phases occurs in the relaxor-ferroelectric systems $\text{Pb}(\text{Mg}, \text{Nb}, \text{Ti})\text{O}_3$ due to internal strain, and are proposed to be intrinsic to the system. [26] Distortion from $Fd\bar{3}m$ to $I4_1/amd$ symmetry, driven by orbital ordering, occurs

in the related spinel compounds NiCr_2O_4 and CuCr_2O_4 . This is followed by further distortion to $Fddd$ symmetry due to magnetostructural coupling.[27] The magnetostructural distortions of NiCr_2O_4 and CuCr_2O_4 are of the same order of magnitude as the structural distortions we observe in MgCr_2O_4 and ZnCr_2O_4 . We can then consider that while tetragonal distortion alone may be sufficient to lift spin degeneracy in MgCr_2O_4 and ZnCr_2O_4 , magnetostructural coupling could then drive further distortion from tetragonal to orthorhombic symmetry. Although kinetics play a minor role in displacive transitions, the low temperatures of spin-Jahn-Teller distortions in MgCr_2O_4 and ZnCr_2O_4 could contribute to stabilizing the metastable two-phase system reported here, preventing the emergence of a true ground state.

In summary, we report coexisting $I4_1/amd$ and $Fddd$ phases in the spin-Jahn-Teller structures of MgCr_2O_4 and ZnCr_2O_4 . Nearly equal phase fractions of the $I4_1/amd$ and the $Fddd$ phase coexist below T_N . The tetragonal phases have larger coherence lengths than the orthorhombic phases. Understanding material structure in these canonically frustrated systems has important consequences for unravelling their degenerate ground states wherein interesting physics is predicted and novel functional states may exist.

We thank Jason Douglas for helpful discussions. MCK is supported by the Schlumberger Foundation Faculty for the Future fellowship. PTB is supported by the National Science Foundation Graduate Research Fellowship program. MWG is supported by a NSERC Postgraduate Scholarship and an International Fulbright Science & Technology Award. RS, MCK, and PTB acknowledge the support of the NSF through the DMR 1105301. YIK is supported by National Research Foundation of Korea (2012-0002868). We acknowledge the use of shared experimental facilities of the Materials Research Laboratory: an NSF MRSEC, supported by NSF DMR 1121053. The 11-BM beamline at the Advanced Photon Source is supported by the DOE, Office of Science, Office of Basic Energy Sciences, under Contract No. DE-AC0206CH11357.

* Electronic address: kemei@mrl.ucsb.edu

- [1] S.-H. Lee, C. Broholm, T. H. Kim, W. Ratcliff, and S.-W. Cheong, Phys. Rev. Lett. **84**, 3718 (2000).
- [2] O. Tchernyshyov, R. Moessner, and S. L. Sondhi, Phys. Rev. Lett. **88**, 067203 (2002).
- [3] S.-H. Lee, G. Gasparovic, C. Broholm, M. Matsuda, J.-H. Chung, Y. J. Kim, H. Ueda, G. Xu, P. Zschack, K. Kakurai, et al., J. Phys.: Condens. Matter **19**, 145259 (2007).
- [4] I. Kagomiya, H. Sawa, K. Siratori, K. Kohn, M. Toki, Y. Hata, and E. Kita, Ferroelectrics **268**, 327 (2002).
- [5] J. D. Dunitz and L. E. Orgel, J. Phys. Chem. Solids **3**, 20 (1957).
- [6] T. Rudolf, C. Kant, F. Mayr, J. Hemberger, V. Tsurkan, and A. Loidl, New J. Phys. **9**, 76 (2007).
- [7] A. P. Ramirez, Annu. Rev. Mater. Sci. **24**, 453 (1994).
- [8] H. Ueda, H. Mitamura, T. Goto, and Y. Ueda, Phys. Rev. B **73**, 094415 (2006).
- [9] L.-S. Martin, A. J. Williams, C. D. Gordon, S. Klemme, and J. P. Attfield, J. Phys.: Condens. Matter **20**, 104238 (2008).
- [10] M. T. Rovers, P. P. Kyriakou, H. A. Dabkowska, G. M. Luke, M. I. Larkin, and A. T. Savici, Phys. Rev. B **66**, 174434 (2002).
- [11] J.-H. Chung, M. Matsuda, S.-H. Lee, K. Kakurai, H. Ueda, T. J. Sato, H. Takagi, K. P. Hong, and S. Park, Phys. Rev. Lett. **95**, 247204 (2005).
- [12] R. ValdesAguilar, A. B. Sushkov, Y. J. Choi, S. W. Cheong, and H. D. Drew, Phys. Rev. B **77**, 092412 (2008).
- [13] H. Ehrenberg, M. Knapp, C. Baetz, and S. Klemme, Powder Diffr. **17**, 230 (2002).
- [14] V. N. Glazkov, A. M. Farutin, V. Tsurkan, H.-A. K. von Nidda, and A. Loidl, J. Phys. Conf. Ser. **145**, 012030 (2009).
- [15] B. H. Toby, J. Appl. Crystallogr. **34**, 210 (2001).
- [16] A. C. Larson and R. B. V. Dreele, Los Alamos National Laboratory Report pp. 86–748 (2000).
- [17] B. J. Campbell, H. T. Stokes, and D. E. Tanner, J. Appl. Crystallogr. **39**, 607 (2006).
- [18] K. Momma and F. Izumi, J. Appl. Crystallogr. **41**, 653 (2008).
- [19] B. C. Melot, J. E. Drewes, R. Seshadri, E. M. Stoudenmire, and A. P. Ramirez, J. Phys.: Condens. Matter **21**, 216007 (2009).
- [20] S. E. Dutton, Q. Huang, O. Tchernyshyov, C. L. Broholm, and R. J. Cava, Phys. Rev. B **83**, 064407 (2011).
- [21] S. Klemme, H. O'Neill, W. Schnelle, and E. Gmelin, Am. Mineral. **85**, 1688 (2000).
- [22] S. Klemme and J. V. Miltenburg, Mineral. Mag. **68**, 515 (2004).
- [23] W. H. Baur, Acta Crystallogr., Sect. B: Struct. Sci **30**, 1195 (1974).
- [24] K. Robinson, G. V. Gibbs, and P. H. Ribbe, Science **172**, 567 (1971).
- [25] P. M. Woodward, D. E. Cox, T. Vogt, C. N. R. Rao, and A. K. Cheetham, Chem. Mater. **11**, 3528 (1999).
- [26] B. Noheda, D. E. Cox, G. Shirane, J. Gao, and Z.-G. Ye, Phys. Rev. B **66**, 054104 (2002).
- [27] M. R. Suchomel, D. P. Shoemaker, L. Ribaud, M. C. Kemei, and R. Seshadri, Phys. Rev. B **86**, 054406 (2012).